ACCOUNTS
of chemical research

Nanophotonics and Nanochemistry: Controlling the Excitation Dynamics for Frequency Up- and Down-Conversion in Lanthanide-Doped Nanoparticles

GUANYING CHEN,*,†,‡ CHUNHUI YANG,*,† AND PARAS N. PRASAD*,‡,§

†*School of Chemical Engineering and Technology, Harbin Institute of Technology, Harbin, Heilongjiang 150001, People's Republic of China,* ‡*Institute for Lasers, Photonics, and Biophotonics and Department of Chemistry, University at Buffalo, State University of New York, Buffalo, New York 14260, United States, and* §*Department of Chemistry, Korea University, Seoul 136-701, Korea*

RECEIVED ON SEPTEMBER 19, 2012

CONSPECTUS

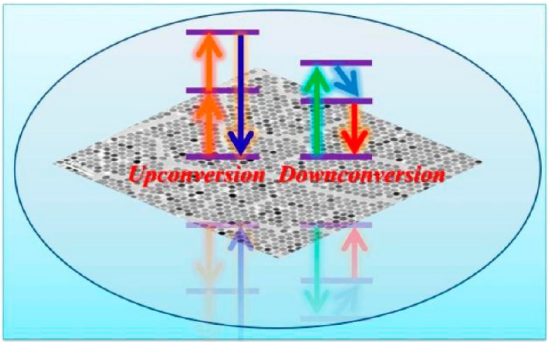

Nanophotonics is an emerging science dealing with the interaction of light and matter on a nanometer scale and holds promise to produce new generation nanophosphors with highly efficient frequency conversion of infrared (IR) light. Scientists can control the excitation dynamics by using nanochemistry to produce hierarchically built nanostructures and tailor their interfaces. These nanophosphors can either perform frequency up-conversion from IR to visible or ultraviolet (UV) or down-conversion, which results in the IR light being further red shifted. Nanophotonics and nanochemistry open up numerous opportunities for these photon converters, including in high contrast bioimaging, photodynamic therapy, drug release and gene delivery, nanothermometry, and solar cells. Applications of these nanophosphors in these directions derive from three main stimuli. Light excitation and emission within the near-infrared (NIR) "optical transparency window" of tissues is ideal for high contrast *in vitro* and *in vivo* imaging. This is due to low natural florescence, reduced scattering background, and deep penetration in tissues. Secondly, the naked eye is highly sensitive in the visible range, but it has no response to IR light. Therefore, many scientists have interest in the frequency up-conversion of IR wavelengths for security and display applications. Lastly, frequency up-conversion can convert IR photons to higher energy photons, which can then readily be absorbed by solar materials. Current solar devices do not use abundant IR light that comprises almost half of solar energy.

In this Account, we present our recent work on nanophotonic control of frequency up- and down-conversion in fluoride nanophosphors, and their biophotonic and nanophotonic applications. Through nanoscopic control of phonon dynamics, electronic energy transfer, local crystal field, and surface-induced non-radiative processes, we were able to produce new generation nanophosphors with highly efficient frequency conversion of IR light. We show that nanochemistry plays a vital role in the design and interface engineering of nanophosphors, providing pathways to expand their range of applications. High contrast *in vitro* and *in vivo* NIR-to-NIR up- and down-conversion bioimaging were successfully demonstrated by our group, evoking wide interests along this line. We introduced trivalent gadolinium ions into the lattice of the nanophosphors or into the shell layer of nanophosphors in a core/shell configuration to produce novel nanophosphors for multimodal (MRI and optical) imaging. We also demonstrate the security and display applications using photopatternable NIR-to-NIR and NIR-to-visible frequency up-conversion nanophosphors with appropriately engineered surface chemistry. In addition, we present preliminary results on dye-sensitized solar cells using up-conversion in fluoride lattice-based nanophosphors for IR photon harvesting.

Published on the Web 01/22/2013 www.pubs.acs.org/accounts
10.1021/ar300270y

1. Introduction

Nanophotonics is an emerging frontier that deals with the interaction of light with matter on a nanometer size scale.[1] The design and control of the excitation dynamics in nanomaterials constitute a major area of nanophotonics; they can be utilized to produce new frequency-converting capabilities in lanthanide-doped nanophosphors.[1−4] Lanthanide-doped nanophosphors are dilute guest−host systems, where trivalent lanthanide ion emitters are dispersed as guests in an appropriate dielectric host lattice. They have captured attentions worldwide recently due to their versatile up or down frequency-converting capabilities utilizing a low-energy continuous-wave (cw) excitation provided by inexpensive diode lasers.[5−9] Through a judicious selection of one or more lanthanide dopants, nanophosphors can display either frequency up-conversion (UC), such as infrared (IR) to shorter wavelength near-infrared (NIR), visible, or ultraviolet (UV), or down-conversion (DC), such as IR being further red-shifted. Unlike the quantum-confined system, the electronic energy gap of lanthanide-doped nanophoshpors does not change with a change in the size or shape.[1] However, their emission properties (color, efficiency, and lifetime) are indeed dependent on nanoscale structures of nanophosphors, which influence the electron−phonon coupling, local crystal field, and nanoscopic ion−ion interactions. Manipulation of a nanoscale dielectric environment to control the excitation dynamics is, therefore, of great importance in order to control their frequency-converting capabilities.

The size, shape, and surface of lanthanide-doped nanophosphors are important in relation to a specific application, while their composition and the local dielectric environment are essential for their excitation dynamics.[1] Owing to the high surface-to-volume ratio of nanophosphors, most of the lanthanide dopants are exposed to surface deactivations caused by surface lattice defects and dangling bonds, as well as by surrounding ligands and solvents that possess high phonon energy. The deactivation can occur directly or through an indirect pathway involving energy migrations from the interior lattice points to the surface sites. Hence, the excitation dynamics is also coupled to the surface properties of nanophosphors due to these nanosize-induced surface effects, which are not so pronounced in bulk crystals. These factors create interests to synthesize nanophosphors of stoichiometric composition in a precisely controlled way and to tailor their interface to generate highly efficient nanophosphors for a specific frequency conversion. Furthermore, tailoring the interface is also important for the colloidal solubility of nanophosphors.

Nanochemistry deals with the confinement of chemical reactions on nanometer length scale to produce materials that are of nanometer dimensions.[1,2] Furthermore, nanochemistry is able to offer the advantage of surface functionalization of nanostructures to make them dispersible in a wide variety of media (e.g., water, polymer, biological fluids).[1,3] Utilizing solution-phase-based colloidal nanochemistry, we show that we are able to fabricate nanophoshors with different composition, size, and shape; here, we utilize a subtle control of their precursors or reaction conditions in a carefully chosen solvent, together with an appropriate surface capping ligand. The ability to precisely control their composition allows us to manipulate their excitation dynamics, while tailoring the interface enables us to make photopatternable and phase-transferred nanophosphors. In addition, we use seed-mediated growth nanochemistry to build hierarchical core/shell nanophosphors to minimize surface-related deactivations and to incorporate multifunctionality at nanoscale. In this Account, we summarize recent progress we have made on nanocontrol of frequency up- and down-conversion in fluoride lattice-based nanophosphors as well as on their biophotonic and nanophotonic applications.

2. Nanocontrol of Excitation Dynamics for Frequency Up- and Down-Conversion

Luminescence in nanophosphors doped with trivalent lanthanide ions generally arises from 4f−4f orbital electronic transitions, with concomitant wave functions localized within a single lanthanide ion.[1] The shielding of 4f electrons by the outer complete 5s and 5p shells results in nonblinking and line-like sharp emissions, which exhibit high resistance to photobleaching and photochemical degradation. Strictly speaking, the main intra-4f electronic dipole transitions of lanthanide ions are forbidden by quantum mechanical selection rules; however, they are still manifested due to local crystal field induced intermixing of the f states with higher electronic configurations.[10,11] A nanostructure control of the local environment surrounding lanthanide ions, thus, will have important manifestations in defining optical properties of nanophosphors. The dipole-forbidden nature of the 4f−4f transition yields very long lifetimes for these energy levels of lanthanide ions. This long lifetime plays an important role in increasing the probability of sequential excitations in the excited states of a single lanthanide ion, as well as in permitting favorable ion−ion interactions in the

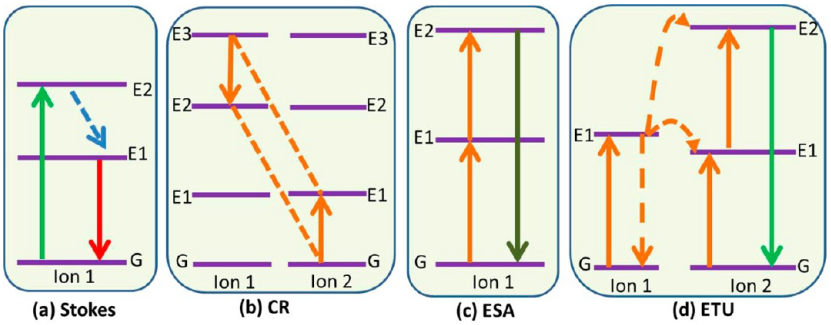

FIGURE 1. Mechanisms of (a) down-conversion, (b) cross relaxation, (c) excited state absorption, and (d) energy transfer up-conversion.

excited states to allow energy transfers between two or more lanthanide ions. Our major focus is to use nanocontrol of local dielectric environment around a lanthanide ion, electron–phonon coupling, ion–ion interactions, and surface-related relaxations, in order to judiciously manipulate frequency down- or up-conversion properties of nanophosphors.

2.1. Schemes of Up- and Down-Conversion. Down-conversion (DC) is a Stokes-shifted emission from an excited lanthanide ion embedded in a host lattice, as illustrated in Figure 1a. A lanthanide ion, excited from the ground state G to the E_2 state, can relax nonradiatively to level E_1 from which a DC emission is produced. The DC process is a single ion process, independent of ion concentration. The nonradiative relaxation from the E_2 to E_1 state is a multiphonon-assisted process that is governed by the phonon dynamics of the nanophosphor.[12] An increase of the lanthanide ion concentration above a certain level induces ion–ion interactions whereby ion 1 can transfer part of its excited energy to ion 2 through a cross relaxation (CR) process of E_3(ion 1) + G(ion 2) → E_2(ion 1) + E_1(ion 2) (Figure 1b). Ion 1 and ion 2 can be of the same type or different, and ion 2 can also be in its excited state in some cases. CR is the main reason for the well-known "concentration quenching mechanism" of Stokes emission. However, CR can be intentionally used to tune the color output in a nanophosphor by enhancing emission from one excited level, while quenching it from another.

Up-conversion (UC) is an anti-Stokes process that converts the absorbed lower energy light, usually in the NIR range, into photoluminescence (PL) of higher energy in UV, visible, or shorter NIR ranges.[8] Because of the involvement of real intermediate energy levels for up-conversion in lanthanides, UC is much more efficient than the nonlinear multiphoton absorption induced up-converted fluorescence where the intermediate levels are virtual.[13] UC in nanophosphors can occur mainly by two fundamental mechanisms: (i) excited state absorption (ESA) (Figure 1c); (ii) energy transfer up-conversion (ETU) (Figure 1d).[1] In the case of ESA, excitation involves successive absorption of pump photons by a single ion due to the ladder-like structure of a simple three-level system. This mechanism requires a nearly equal separation from G to E_1 and E_1 to E_2, as well as the reservoir capability (the long lifetime) of the intermediate level of E_1. The emission from E_2 to G finally occurs to produce UC. In an ETU process, ion 1, known as a sensitizer, is first excited from the ground state to its metastable level E_1 by absorption of a pump photon; it then transfers its harvested energy to the ground state G and the excited state E_1 of ion 2, known as an activator. These processes produce excitation of ion 2 to its upper-emitting state E_2. The UC efficiency of an ETU process is strongly dependent on the average distance between the neighboring sensitizer–activator pair, which is determined by the dopant concentration. In contrast to ETU, the efficiency of an ESA process is independent of the dopant concentration, because ESA involves sequential excitation in the same ion.

2.2. Nanocontrol of Excitation Dynamics for UC and DC PL. In order to realize efficient UC or DC emissions in lanthanide-doped nanophosphors, we utilized five strategies, as illustrated in Figure 2, to manipulate the excitation dynamics, which are discussed below.

2.3. Nanoscopic Control of Phonon Dynamics. It is well-known that phonon-induced nonradiative processes are the main loss mechanisms for both UC and DC emissions; the luminescence efficiency is quite sensitive to the distribution of phonon density of states in the lattice of a nanophosphor. These nonradiative processes involve multiphonon-assisted relaxations, whereby the energy difference between the higher and the lower energy levels is converted into many lattice phonons.[12] Generally, the larger the number of phonons needed to convert the excitation energy into phonon energy, the lower is the efficiency of the nonradiative process. Hence, to enhance the emission efficiency by

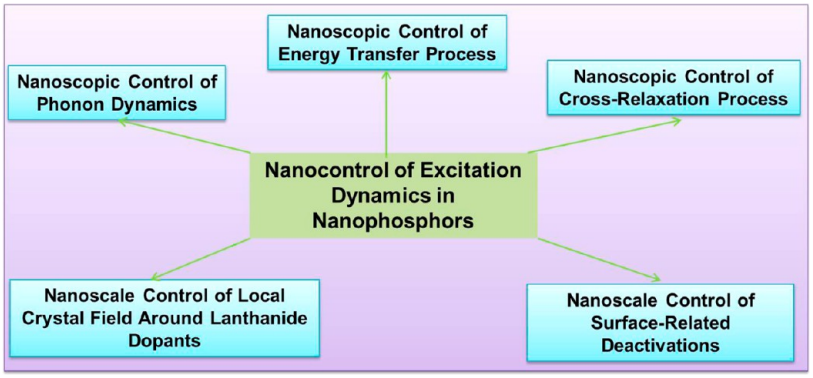

FIGURE 2. Our strategies for nanocontrol of the excitation dynamics in lanthanide-doped nanophosphors.

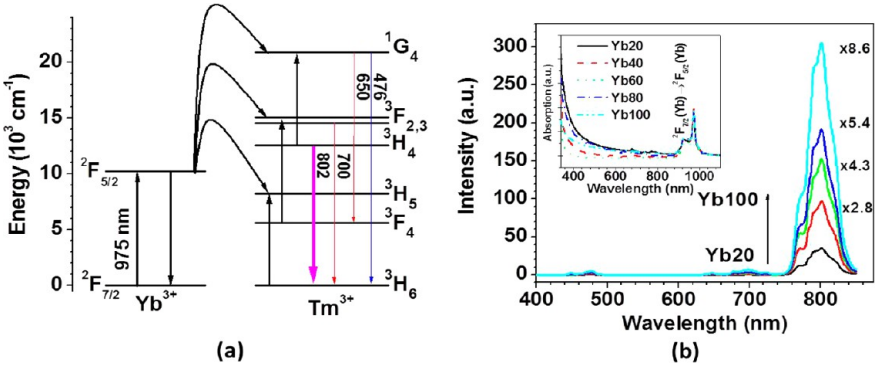

FIGURE 3. (a) Energy levels of Yb^{3+} and Tm^{3+} and (b) UC PL spectra of colloidal cubic $NaYF_4$ nanocrystals doped with 2% Tm^{3+} and 20−100% Yb^{3+}; excitation at ~975 nm.

reducing nonradiative rate, it is desirable to have the lanthanide ions incorporated into a dielectric host of very low frequency phonons. Among investigated host materials of nanophosphors, fluoride materials have the lowest phonon cutoff energy and generally exhibit the highest UC or DC efficiency due to minimization of nonradiative losses in the intermediate states or the emitting states. In addition, when taking into account the strength of electron−phonon coupling and the phonon density of states, theoretical calculations by Auzel et al. indicate that the UC efficiencies of the green and blue emissions with the Yb^{3+}/Er^{3+} and Yb^{3+}/Tm^{3+} materials have a maximum at phonon energy of ~380 cm^{-1}, well matching the lattice vibrations of fluoride materials (e.g., ~350 cm^{-1} for $NaYF_4$ host lattice).[9] Hence, we employ fluoride-based nanoparticles to realize high UC or DC efficiencies, as can be seen in the examples in sections 2.4−2.7. Another reason for the selection of fluoride host lattices is their robust chemical- and photostability.

2.4. Nanoscopic Control of Energy Transfer Process. Energy transfer is important for ETU mechanisms such as in the Yb^{3+}/Tm^{3+}, Yb^{3+}/Er^{3+}, and Yb^{3+}/Ho^{3+} mixed systems, which are identified to be the most efficient ion pairs for up-conversion at ~980 nm.[8] The nonradiative energy transfer mainly involves multipolar or exchange interactions between two lanthanide ions; these interactions are strongly dependent on the ion-pair distance, which can be manipulated by the lanthanide dopant concentration.[1,9] However, the CR process, detrimental to luminescent efficiency, also becomes pronounced at a high lanthanide dopant concentration. This sets a limit on increasing lanthanide concentration to shorten the ion−ion distance for manipulating the energy transfer process in order to achieve a high efficiency. However, it is important to note that, unlike the activator ions of Tm^{3+}, Er^{3+}, and Ho^{3+}, the sensitizer Yb^{3+} ion has one exclusive excited energy level of the $^2F_{5/2}$ state produced by the absorption at ~980 nm (Figure 3a).[8] The variation of its concentration generally does not induce a CR process, thus excluding any "concentration quenching effect". Figure 3 shows that, through control of the Yb^{3+} concentration, we can easily manipulate the energy transfer rate between Yb^{3+} and Tm^{3+} and realize efficient NIR-to-NIR UC PL in Yb^{3+}/Tm^{3+}-codoped $NaYF_4$ nanophosphors.[14]

2.5. Nanoscopic Control of the CR Process. The CR process responsible for concentration quenching generally

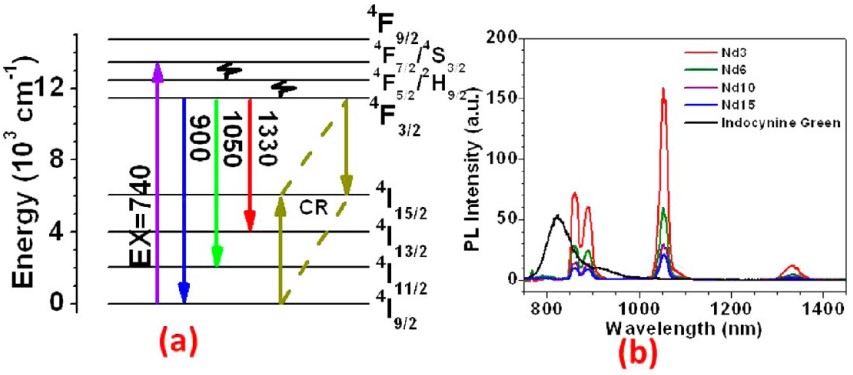

FIGURE 4. (a) Mechanism for the observed NIR PL emission in Nd^{3+}, when excited at 740 nm and (b) PL from the colloidal $NaGdF_4$ nanocrystals doped with 3%, 6%, 10%, and 15% Nd^{3+} and from the reference standard of indocyanine green.

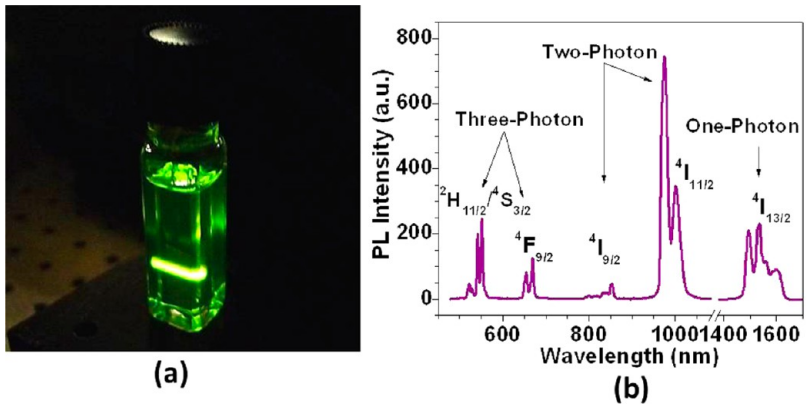

FIGURE 5. (a) Photographic image of UC PL in 1 wt % colloidal $LiYF_4$:10% Er^{3+} nanocrystals under unfocused laser excitation at 1490 nm of 4 W/cm^2 and (b) calibrated PL spectra of colloidal $LiYF_4$:10% Er^{3+} nanocrystals under laser excitation at 1490 nm.

plays a crucial role in a DC process; it also impacts the UC efficiency when increasing the concentration of activators such as Tm^{3+}, Er^{3+}, and Ho^{3+}. As discussed above, the CR process is dependent on the ion−ion distance, which is determined by the dopant concentration in a nanophosphor. With respect to Nd^{3+}-containing nanocrystals, the CR process of $^4F_{3/2} + {}^4I_{9/2} \rightarrow 2{}^4I_{15/2}$ nonradiatively depopulates the excited $^4F_{3/2}$ level, which adversely affects the PL intensity by concentration quenching (Figure 4a).[15] A reduction in the concentration of the doped Nd^{3+} ions can maximize the PL quantum yield due to a decrease in the CR process because of a longer Nd^{3+}−Nd^{3+} distance. As illustrated in Figure 4b, the QY increases with a decrease in the concentration of Nd^{3+}. The highest QY is about 22%, observed in the nanocrystals of $NaGdF_4$: 3% Nd^{3+}.[15] Although CR in UC is not explicitly discussed in this Account, an optimum concentration of the activator (Tm^{3+}, Er^{3+}, and Ho^{3+}) is determined to be generally below 2% in the sensitizer/activator systems of Yb^{3+}/Tm^{3+}, Yb^{3+}/Er^{3+} and Yb^{3+}/Ho^{3+} to yield high UC efficiency.[8]

2.6. Nanoscale Control of the Local Crystal Field around Lanthanide Dopants. The local crystal field of a host material surrounding a lanthanide site has an important influence on the luminescence efficiency of the lanthanide emitter, because the local crystal symmetry around the lanthanide ion determines its optical properties. A less symmetric crystal phase is generally favorable for higher UC efficiency, since intermixing of the lanthanide ion's f states with higher electronic configurations can be more pronounced.[10,11] It has been shown that hexagonal $NaYF_4$:Yb^{3+}/Er^{3+} microcrystals exhibit visible UC PL that is 4.4 times higher than its cubic counterparts,[16] and monoclinic ZrO_2:Er^{3+} nanoparticles emit higher UC PL than the tetragonal form.[17] A nanostructure control of the local crystal field through selecting appropriate nanocrystalline phases or modifications of a specific crystal field through dopant-induced Columb interactions[18] is important in order to obtain a high UC efficiency. For example, we use the $LiYF_4$:Er^{3+} nanoparticles of the tetragonal scheelite ($CaWO_4$) phase to realize efficient conversion of telecomm wavelength at

1490 nm.[19] The unique local crystal field at the Er^{3+} site (by partial substitution of Y^{3+} ions) of the low S_4 point symmetry, leads to an extremely long lifetime for the intermediate metastable states of Er^{3+} ions (~10 ms) and a large absorption cross section at the excitation wavelength, which are important for highly efficient UC PL (Figure 5). The efficiency can be quantitatively evaluated using up-conversion quantum yield (UCQY), which is defined as the ratio of the number of emitted up-converted photons to the number of absorbed NIR photons. The total quantum yield for the visible and the NIR emission is 1.2% ± 0.1% under 1490 nm excitation of 150 W/cm^2,[19] almost 4 times higher than the highest UCQY reported for the 100 nm sized hexagonal $NaYF_4$:20% Yb^{3+}/2%Er^{3+} nanocrystals under ~980 nm excitation of 150 W/cm^2.[20]

2.7. Nanoscale Control of Surface-Related Deactivation in Nanophoshors. Although nanophosphors with small sizes are able to be synthesized using nanochemistry (see section 3), the resulting nanophosphors generally have a low PL QY, because they expose numerous lanthanide dopants to surface deactivations resulting from the high surface-to-volume ratio at nanometer dimensions.[20] Surface-related deactivations are manifested in two ways: (1) excited dopants located on or around the surface can be deactivated directly by neighboring quenching centers; (2) the energy contained in dopants located in the center of nanophosphors can migrate a long distance to the dopant on/around surface or directly to the surface quenching sites (Figure 6a). This second way is more prominent for UC nanophosphors, because a high sensitizer concentration of Yb^{3+} (more than 18%) is often introduced into nanophosphors doped with Yb^{3+}/Tm^{3+}, Yb^{3+}/Er^{3+}, or Yb^{3+}/Ho^{3+} to achieve a high UC PL.[8] The long distance transportation of energy in a Yb^{3+} sublattice is due to the unique two-energy-level structure of Yb^{3+} in association with its long-lived excited state (Figure 3a). We note that the harvested UV energy can travel 5 nm with no losses through a Gd^{3+} sublattice in the $NaGdF_4$ host lattice.[4] In an analogy, the absorbed NIR energy in a Yb^{3+} sublattice might be able to travel several or even tens of nanometers in nanophososphors with a high Yb^{3+} concentration. Hence, the surface-related quenching mechanisms in these nanophosphors pose an important challenge, which we address by using the epitaxial growth of an inert outer shell layer on the nanoparticle to reduce the imperfections in the surface lattice and to shield the core from the ligands and solvents of high phonon energy. Indeed, we find that the QY of DC PL in the 11 nm

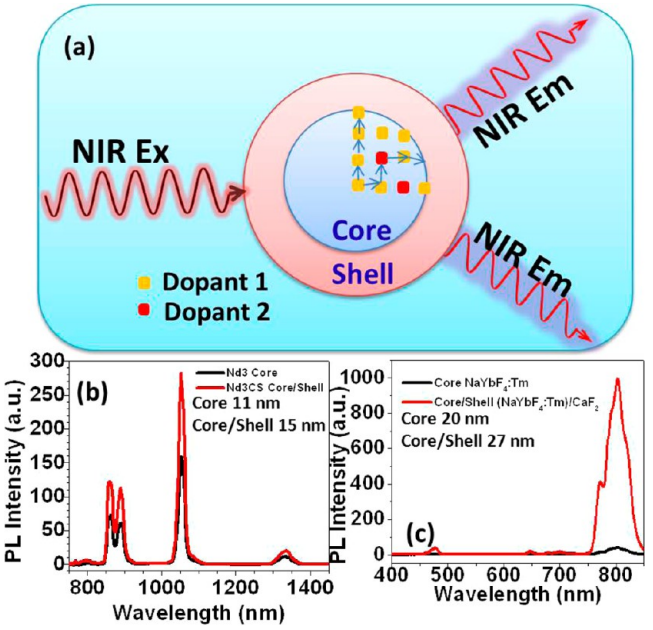

FIGURE 6. (a) Schematics of core/shell structure and random energy migration between lanthanide ions in the core nanoparticles, (b) DC PL of the colloidal $NaGdF_4$:3% Nd^{3+} core and the ($NaGdF_4$:3% Nd^{3+})/$NaGdF_4$ core/shell nanophosphors under laser excitation at 740 nm, and (c) UC PL of the α-$NaYbF_4$:0.5% Tm^{3+} core and the α-($NaYbF_4$:0.5% Tm^{3+})/CaF_2 core/shell nanoparticles. The absorptions of the core and the core/shell nanoparticles have been normalized at the excitation wavelength via adjusting their concentrations.

$NaGdF_4$:3% Nd^{3+} nanoparticles is increased twice by growing a thin layer of $NaGdF_4$ shell of 2 nm (Figure 6b).[15] Similarly the QY of UC PL in the 18 nm sized α-$NaYbF_4$:0.5% Tm^{3+} core nanoparticles is increased by 39 times due to the epitaxial growth of a perfect CaF_2 shell, leading the QY of NIR-to-NIR UC PL to be as high as 0.6% under low energy excitation of 0.3 W/cm^2 (Figure 6 c).[21] The difference of the enhancement factor between UC and DC PL QY confirms a more pronounced energy relaxation in UC due to Yb^{3+}-sublattice-mediated energy migration from the interior lattice points to the surface quenching sites.

3. Nanochemistry

Nanochemistry lends itself to a precise control of synthetic parameters to produce monodispersed nanoparticles or to hierarchically build nanostructures. It generally utilizes either traditional chemical synthesis in the solution phase under nanoconfined geometries (as in micelles and reverse micelles) or termination of reaction at a precise point of growth (chemical capping).[1,3] Nanochemistry is also able to offer the advantage of surface functionalization of nanostructures of different types for different purposes. Figure 7

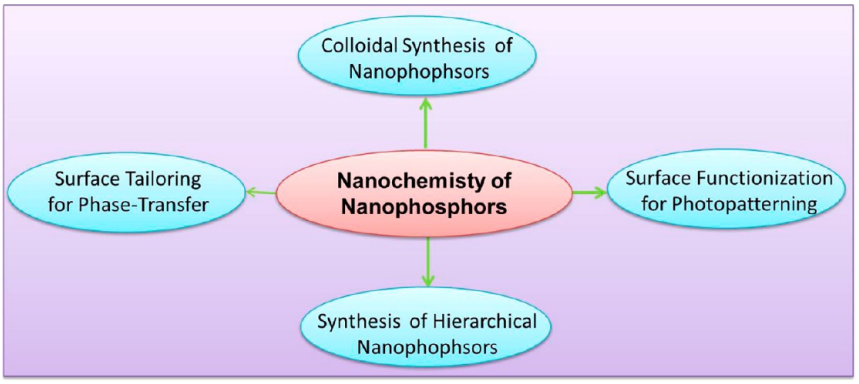

FIGURE 7. Nanochemical approaches for lanthanide-doped nanophosphors.

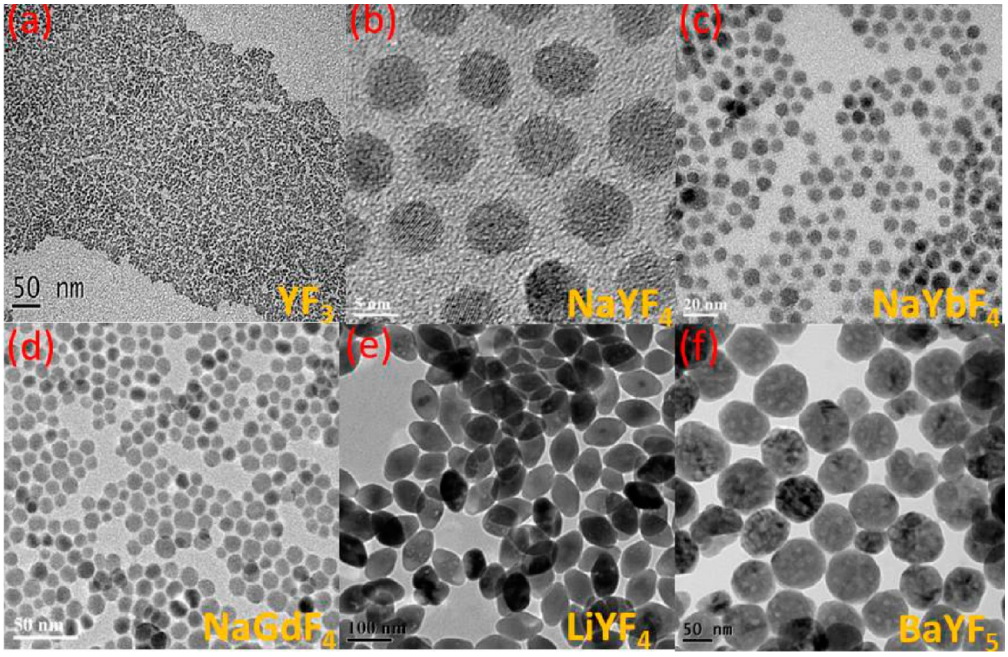

FIGURE 8. TEM images of nanocrystals of (a) YF_3:10%Yb^{3+}/1%Er^{3+}, (b) $NaYF_4$:20% Yb^{3+}/2%Tm^{3+}, (c) $NaYbF_4$:2% Tm^{3+}, (d) $NaGdF_4$:3% Nd^{3+}, (e) $LiYF_4$:10% Er^{3+}, and (f) $BaYF_5$:20% Yb^{3+}/2% Er^{3+}.

displays examples of various types of nanochemistry for lanthanide-doped DC and UC nanophosphors, which are discussed below in different subsections.

3.1. Controlled Synthesis of Lanthanide-Doped UC and DC Nanocrystals. Figure 8 shows UC or DC nanophosphors of different types, with varying size, shape, or phase. Examples shown here are (a) 3.7 nm orthorhombic YF_3,[22] (b) 7 nm cubic $NaYF_4$,[14] (c) 10 nm cubic $NaYbF_4$,[14] (d) 10 nm hexagonal $NaGdF_4$ nanophosphors,[15] (e) 85 nm tetragonal $LiYF_4$,[19] and (f) 60 nm tetragonal $BaYF_5$ nanoparticles.[23] These lanthanide-doped nanophosphors were synthesized using solution-based colloidal nanochemistry via three types of synthetic approaches: (i) thermal decomposition method (Figure 8a−c,e); (ii) Ostwald-ripening method (Figure 8d); (iii) hydrothermal method (Figure 8f). The details of these three synthetic approaches are described in the Supporting Information.

3.2. Seed-Mediated Epitaxial Growth of Hierarchical Core/Shell Nanophosphors. We use a stepwise seed-mediated growth technique to grow a shell layer on the core nanoparticle to reduce surface-related quenching mechanisms or to incorporate a functional shell at nanoscale for bioimaging use (e.g., $NaGdF_4$ for MRI). The first step produces core nanophosphors utilizing appropriate nanochemistry described in section 3.1, which are then used as seeds in the second step to induce further epitaxial growth. To create a homogeneous interface between the core and the outer shell to minimize lattice defects and strain, the host

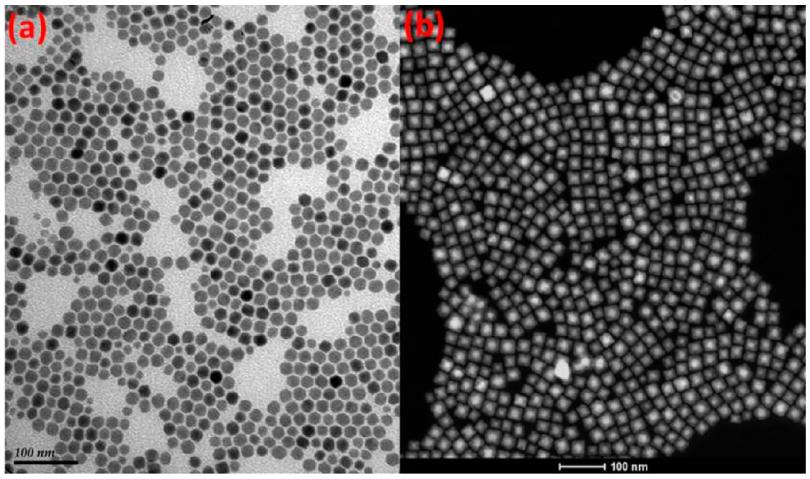

FIGURE 9. (a) TEM image of the α-$NaYbF_4$:0.5% Tm^{3+} core and (b) high-angle annular dark-field scanning transmission electron microscopy image of the (α-$NaYbF_4$:0.5% Tm^{3+})/CaF_2 nanoparticles with resolved core/shell structures; both the core (bright) and the shell (dark) are clearly visible.

material of the shell should exhibit a small lattice mismatch with the core materials. We have successfully prepared core/shell nanocrystals of UC ($NaYbF_4$:2%Tm^{3+})/$NaGdF_4$,[24] (YF_3:Yb^{3+}/Er^{3+}/Tm^{3+})/YF_3,[22] and α-($NaYbF_4$:0.5% Tm^{3+})/CaF_2[21] (Figure 9) and DC ($NaGdF_4$:3% Nd^{3+})/$NaGdF_4$.[15]

3.3. Surface Tailoring of Nanophosphors for Phase Transfer. The resulting UC or DC nanophosphors in section 3.1 and the core/shell nanoparticles in section 3.2 are generally hydrophobic, because they are capped by long-chain hydrophobic ligands, for example, oleic acid. We have employed three simple approaches for engineering the interface of nanophosphors to allow their dispersion in aqueous phase. (i) Ligand exchange with short-chain acids, for example, 3-mercaptopropionic acid (MPA) in which the thiol group is chelated with surface metal ions of the nanophosphor, while the carboxylic group is pointing outside.[25] MPA not only permits aqueous dispersion of nanophosphors but also provides unused carboxylic group sites on the surface for linking an antibody (e.g., anti-claudin 4).[26] (ii) Salinization to produce silica coating. (iii) Ligand-free method.[15] The removal of oleic acid from the nanoparticle surface is through a direct acid treatment with the assistance of sonication.[27] The details of the pertinent chemistry and procedure are described in the Supporting Information.

3.4. Surface Functionalization of Nanophosphors for Photopatterning. The synthesized nanophosphors are neither photopatternable nor homogenously dispersible in polymers due to a lack of appropriate functional ligand on the surface. To allow photopatterning of nanophosphors for security use, we utilize ligand exchange with a unique functional ligand that has an acid-labile moiety, that is, *t*-butoxycarbonyl (*t*-BOC).[28] The acid-labile moiety enables the *t*-BOC ligand to be shortened and thus the solubility of the nanophosphors in a polymer to be changed by UV illumination in the presence of a photoacid-generating compound (PAG). The nanophosphors in UV-exposed parts are subsequently unable to redisperse in an organic solvent such as hexane (Figure 10). Thus, the developer solution of anhydrous hexane removes only the unexposed portions of the film, creating well-photopatterned nanophosphors.[28] The security application of these nanophosphor patterns will be discussed in section 4.3.

4. Nanophotonic and Biophotonic Applications

Owing to their unique optical and chemical properties, UC or DC nanophosphors find a broad range of applications,[5−9] as illustrated in Figure 11. In this paper, we provide some examples from our recent results on NIR-to-NIR UC and DC PL imaging; multimodal bioimaging; security and displays; and solar cells.

4.1. Optical Imaging. 4.1.1. NIR-to-NIR UC PL Bioimaging. In this section, we display the use of NIR-to-NIR UC in Tm^{3+}/Yb^{3+}-codoped fluoride nanophosphors for bioimaging (emission at ∼800 nm, excitation at ∼975 nm, Figure 12a).[21,25] Both the excitation and the emission wavelengths are within the "optical transparency window" of biological tissues (700−1100 nm),[2,3] which not only allows for deeper light penetration but also results in lower autofluorescence and reduced light scattering. A low-cost cw laser diode is utilized as the excitation source, with an excitation density of $\sim 10^{-1}$ W/cm^2, which is in marked contrast to the use of high excitation density of $\sim 10^6$ W/cm^2 in nonlinear multiphoton imaging.[3,13] When an aqueous

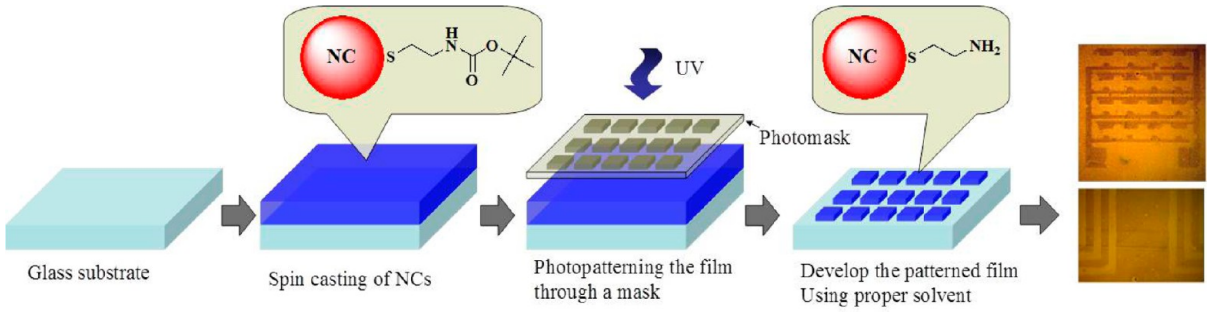

FIGURE 10. Schematic illustration of the chemistry of photopatterning nanophosphors.

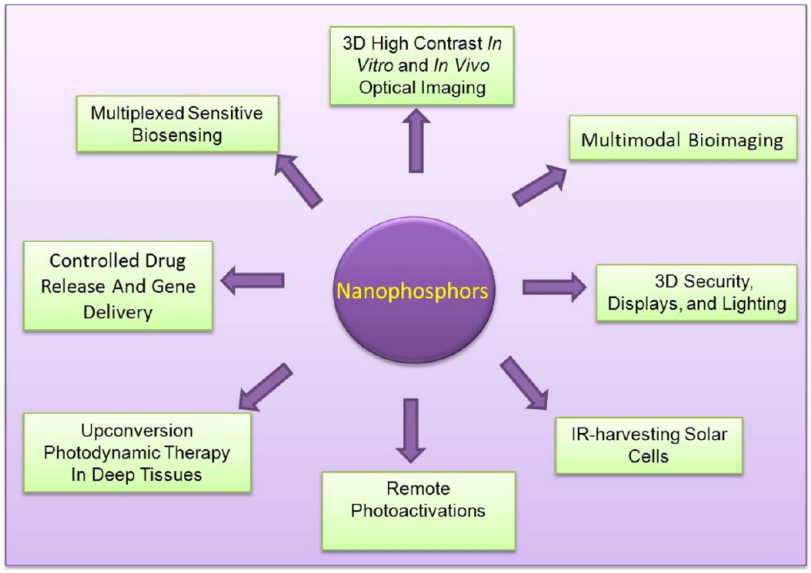

FIGURE 11. The various applications of nanophosphors.

dispersion of nanophophosors of $NaYF_4$:2%Tm^{3+},20% Yb^{3+} is used, a high contrast PL image against the background is observed in the pancreatic cell as well as in whole-body of Balb-c mouse (IV injection) (Figure 12b,c); the signal to background ratio (SBR) is evaluated to be on the order of ~10.[25] To improve the SBR and increase the imaging depth, we then designed α-($NaYbF_4$:0.5% Tm^{3+})/CaF_2 core/shell nanophosphors, which display a QY as high as 0.6% under imaging conditions. The SBR is increased to be as high as 310 (Figure 12d). In addition, utilizing the developed core/shell nanophosphors, we also demonstrated that the imaging depth can reach 3.2-cm in a thick animal tissue (pork), with a high contrast, as shown in Figure 12e,f.[21]

4.1.2. NIR-to-NIR DC PL Bioimaging. We also explored efficient nanophosphors that emit NIR-to-NIR DC PL for high-contrast *in vitro* and *in vivo* bioimaging;[15] they provide the same advantage that the wavelengths of excitation and emission PL are both within the "optical transparency window" of tissues.[2,3] In addition, they have the merit that they can efficiently be excited by an incoherent light source, and the efficiency can be quite high due to one-photon excitation. Through nanocontrol of the excitation dynamics (see sections 2.5 and 2.7), we designed ($NaGdF_4$:3% Nd^{3+})/$NaGdF_4$ nanocrystals in which the NIR PL QY can reach 40% when dispersed in hexane. High contrast imaging of Hela cells (Figure 13b) and nude mouse (Figure 13c) were produced utilizing excitations from an incoherent lamp light source with appropriate filters through the observation of NIR PL at 900 nm.[15]

4.2. Mulitmodal Imaging. Multimodal bioimaging requires combining optical imaging with other imaging modalities. Gd^{3+} ions can efficiently alter the relaxation times of surrounding water protons due to the possession of a large number of unpaired electrons. Thus, Gd^{3+} complexes are widely used as contrast agents in MRI.[2] By doping of Gd^{3+} in UC or DC nanophosphors, a novel nanomaterial possessing the combined advantages of fluorescence and magnetic

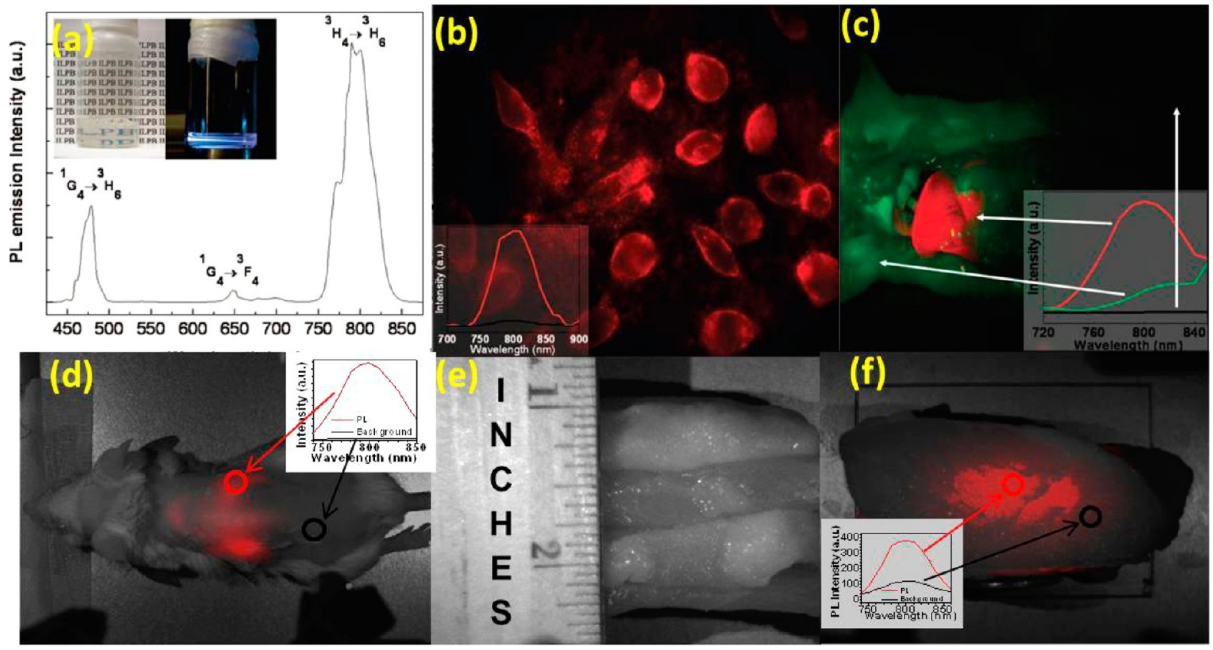

FIGURE 12. (a) PL spectra of the $NaYF_4$:2%Tm^{3+},20%Yb^{3+} UCNPs in aqueous dispersion under excitation at 975 nm, (b) PL images of Panc 1 cells treated with $NaYF_4$:2%Tm^{3+},20%Yb^{3+} UCNPs, (c) body images of a mouse intravenously injected with UCNPs, after dissection, (d) whole body images of a BALB/c mouse injected via tail vein with the hyaluronic acid-coated α-($NaYbF_4$:0.5% Tm^{3+})/CaF_2 core/shell nanophosphors, (e) bright-field image of a pork tissue (side view), displaying the imaging depth, and (f) UC PL image of a cuvette containing α-($NaYbF_4$:0.5% Tm^{3+})/CaF_2 core/shell nanophosphors covered with the pork tissue of panel e.

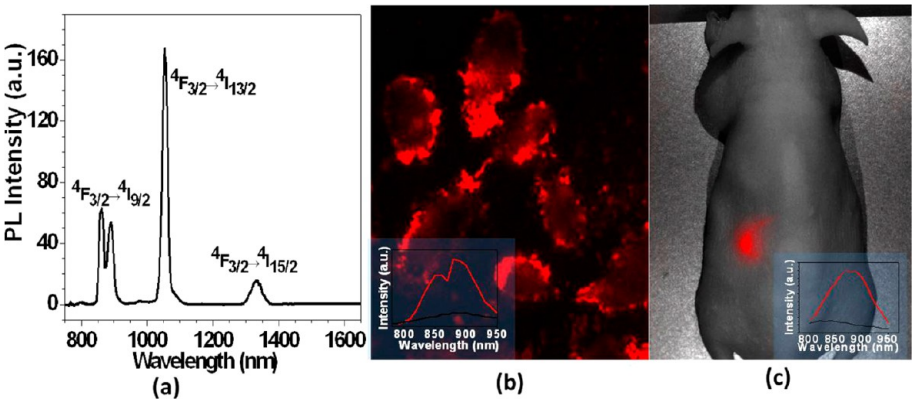

FIGURE 13. (a) PL of core/shell ($NaGdF_4$:3% Nd^{3+})/$NaGdF_4$ nanocrystals, excited at 740 nm, (b) PL images of Hela cells treated with ligand-free ($NaGdF_4$:3% Nd^{3+})/$NaGdF_4$ nanoparticles, and (c) *in vivo* whole body imaging of a nude mouse, subcutaneously injected with ligand-free ($NaGdF_4$:3% Nd^{3+})/$NaGdF_4$ nanocrystals.

properties can be achieved (Figure 14a).[26] We believe that Gd^{3+} ions located around the nanoparticle surface allow a more efficient exchange with the surrounding water protons than the Gd^{3+} ions in the interior of a nanoparticle. Using nanochemisty, we produced poly(acrylic acid)-modified ($NaYbF_4$:2% Tm^{3+})/$NaGdF_4$ core/shell nanocrystals (size, 12 nm) that display an enhanced NIR-to-NIR UC PL and a strong MR signal in which the longitudinal relaxivity value ($1/T_1/Gd^{3+}$) is about 2.6 mM^{-1} s^{-1}.[24] This value is about 10 times higher than that of the MPA-coated and the Gd^{3+}-doped UC nanophosphors of $NaYF_4$:Yb^{3+}/Er^{3+} or DC nanophosphors of $NaYF_4$:Eu^{3+} (size, 25−30 nm).[26] We have not implemented joint *in vivo* MRI imaging and PL imaging yet. However, it has already become a topic that is being widely investigated.[6]

4.3. Security and Displays. NIR-to-NIR and NIR-to-visible UC PL offers an opportunity to produce new security markers, because an encrypted 3D pattern, invisible to us with regular light sources, provides a unique way to secure the object.[28] We exchanged the surface group with a ligand

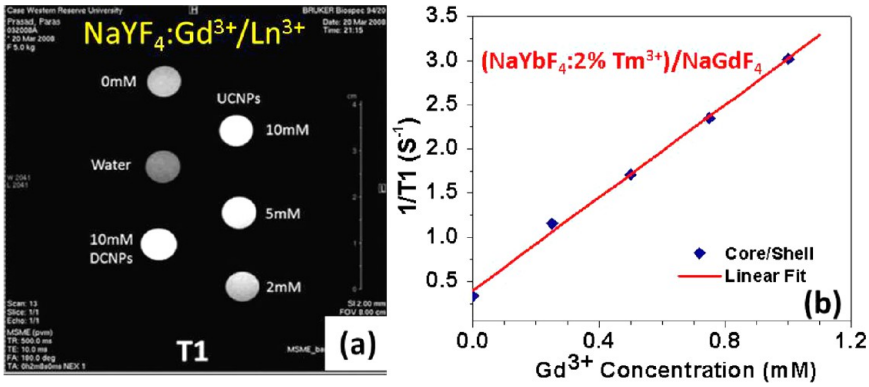

FIGURE 14. (a) T_1 weighted images of nanocrystals of $NaYF_4$:10% Gd^{3+}/10% Eu^{3+} (DCNPs, left column) and $NaYF_4$:10% Gd^{3+}/2% Er^{3+}/10% Yb^{3+} (UCNPs, right column) and (b) plots of $1/T_1$ as a function of gadolinium concentration for poly(acrylic acid)-modified ($NaYbF_4$:2% Tm^{3+})/$NaGdF_4$ UCNPs.

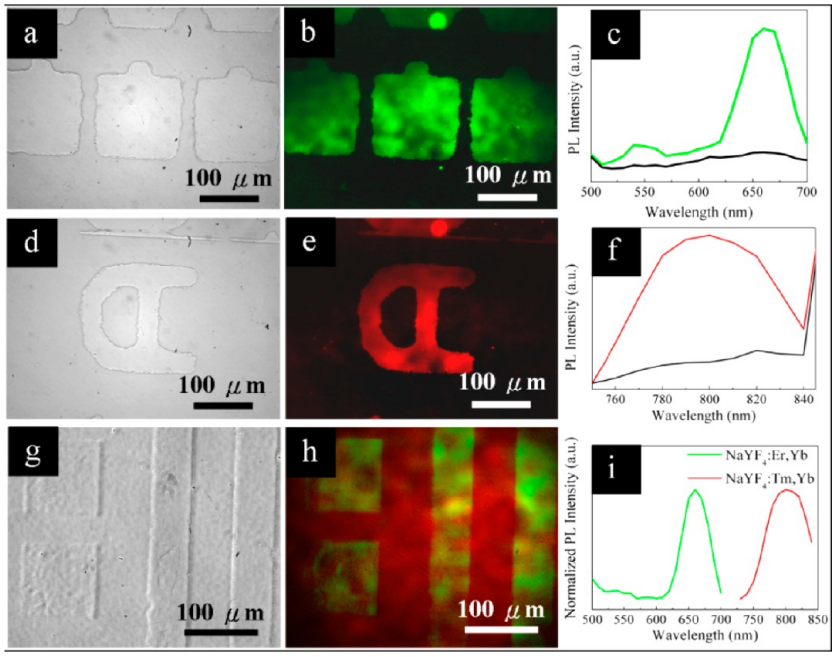

FIGURE 15. Optical microscopic images of patterned NCs and their PL spectra: transmission images of (a) $NaYF_4$:Er/Yb, (d) $NaYF_4$:Tm/Yb, (g) a bilayer of $NaYF_4$:Er,Yb (first layer, patterned) and $NaYF_4$:Tm/Yb (second layer, no pattern); fluorescence images of (b) $NaYF_4$:Er/Yb, (e) $NaYF_4$:Tm/Yb, and (h) merged fluorescence image of both nanophosphors; the localized spectra display the corresponding emission from the patterned area (c, f, i) (green line, $NaYF_4$:Er,Yb; red line, $NaYF_4$:Tm,Yb) and the glass substrate (black line). The excitation wavelength is 975 nm.

containing an acid-labile group as described above (section 3.4) to make $NaYF_4$:Er/Yb and $NaYF_4$:Tm/Yb nanophosphors photopatternable. Through traditional photolithiography, a well-defined nanophosphor pattern with single (Figure 15a,d) or multiple layers (3-D) (Figure 15g), can be easily fabricated. They display either visible (Figure 15c) or NIR (Figure 15f) or both (Figure 15i) UC PL, when excited at 975 nm.[28]

4.4. Solar Cell. A dye-sensitized solar cell (DSSC) is regarded as a promising solar energy converter due to its relatively high efficiency and low cost. However, a lack of appropriate photosensitizers in the IR region significantly limits the improvement in their efficiency.[29] To harvest and make use of light in the IR region, one possible way is to absorb the IR light for visible photon up-conversion, the energy of which can then be radiatively (light energy transfer, LET) or nonradiatively (Föster resonance energy transfer, FRET) transferred to the dye sensitizer. We use this energy relay of the IR light in a DSSC as illustrated in Figure 16a. The $I-V$ characteristics show a prominent increment in the photocurrent with an increase in the irradiation power at ~980 nm at which the absorption of UC nanophosphors is

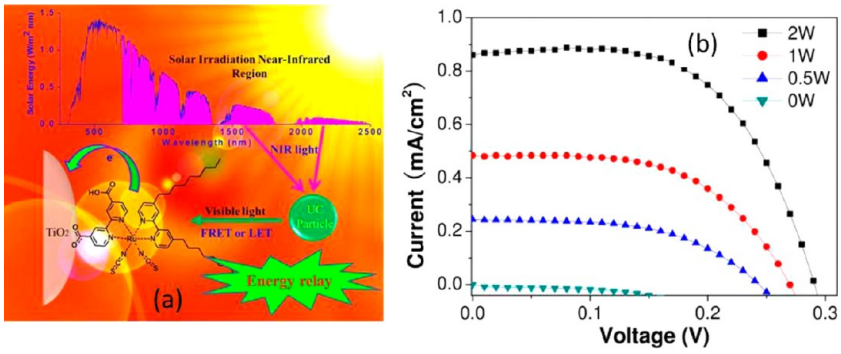

FIGURE 16. a) Schematic illustration for energy relay of IR solar light in dye-sensitized solar cells (the sensitizer dye, Z907) using UC nanophosphors; (b) *I*−*V* characteristics of a dye-sensitized solar cell with the addition of 20 nm sized hexagonal $NaYF_4$:Yb^{3+}/Er^{3+} UC nanophosphors under the illumination of a 980 nm laser.

located (Figure 16b). This result indicates that the improved photocurrent derives from the energy relay process between the UC nanophosphors and the sensitizer, Z907 dye.[29]

5. Conclusion and Perspectives

This Account summarizes our recent developments using nanophotonics and nanochemistry to produce new generation photon converters. These lanthanide-doped UC or DC nanophosphors exhibit promising potential applications in high-contrast *in vitro* and *in vivo* bioimaging, multimodal imaging, security and displays, and solar cells. However, there are still a number of challenges to be overcome for their practical use. These challenges are as follows: (1) The extinction of nanophosphors (UC and DC) is low and narrow. This drawback is an intrinsic feature of 4f−4f optical transitions in lanthanide ions. An antenna effect from dyes, plasmonic coupled structures, quantum dots, or other doping elements with a strong absorption may be of great help in this direction. (2) The quantum yield of nanophosphors is still low, in particular, under low excitation density of 10^{-2} to 10^{-1} W/cm^2. A manipulation of the local environment around the lanthanide dopants in nanophosphors may be a promising direction to enhance the quantum yield. (3) The area of frequency down-conversion nanophosphors in the IR range is still in its infancy. It will be of great interest to extend their capability to possess multicolor emissions under single wavelength excitation and mutifunctionality for multimodal imaging.

This work was supported in part by the grants from the Air Force Office of Scientific Research (Grant FA 9550-11-1-0121) and Natural Science Foundation of China (Grant 51102066).

Supporting Information. Details of chemistry for synthesis and phase transfers of nanophosphors. This material is available free of charge via the Internet at http://pubs.acs.org.

BIOGRAPHICAL INFORMATION

Guanying Chen received his B.S. and Ph.D. degree in optics from Harbin Institute of Technology in 2004 and 2009, respectively. He is a research assistant professor at the Institute for Lasers, Photonics, and Biophotonics at University at Buffalo, State University of New York. He also holds a joint affiliation with Harbin Institute of Technology.

Chunhui Yang received her B.S. degree in chemistry from Dalian University of Technology in 1991 and obtained M.S. and Ph.D. degrees in chemistry from Harbin Institute of Technology in 1996 and 2001, respectively. She then joined Harbin Institute of Technology as an assistant Professor and was promoted to Associate Professor and Full Professor in 2001 and 2004, respectively.

Paras N. Prasad is a SUNY Distinguished Professor of Chemistry, Physics, Electrical Engineering and Medicine; the Samuel P. Capen Chair of Chemistry; the Executive Director of Institute for Lasers, Photonics, and Biophotonics, University at Buffalo; and a Distinguished Foreign Professor at Korea University. He was named among top 50 science and technology leaders in the world by Scientific American in 2005. He has published nearly 700 scientific and technical papers, four monographs, and eight edited books. He received many scientific awards and honors (Morley Medal; Schoellkopf Medal; Guggenheim Fellowship; Fellow of the APS, OSA, and SPIE).

FOOTNOTES

*E-mail addresses: guanying@buffalo.edu; yangchh@hit.edu.cn; pnprasad@buffalo.edu.
The authors declare no competing financial interest.

REFERENCES

1 Prasad, P. N. *Nanophotonics*; Wiley-Interscience: Hoboken, NJ, 2004.
2 Prasad, P. N. *Introduction to Nanomedcine and Nanobioengineering*; Wiley-Interscience: Hoboken, NJ, 2012.
3 Prasad, P. N., *Introduction to Biophotonics*; Wiley-Interscience: Hoboken, NJ, 2003.
4 Wang, F.; Deng, R.; Wang, J.; Wang, Q.; Han, Y.; Zhu, H.; Chen, X.; Liu, X. Tuning Upconversion through Energy Migration in Core/Shell Nanoparticles. *Nat. Mater.* **2011**, *10*, 968–973.

5 Wang, G.; Peng, Q.; Li, Y. Lanthanide-Doped Nanocrystals: Synthesis, Optical-Magnetic Properties, and Applications. *Acc. Chem. Res.* **2011**, *44*, 322–332.

6 Zhou, J.; Liu, Z.; Li, F. Upconversion Nanophosphors for Small-Animal Imaging. *Chem. Soc. Rev.* **2012**, *41*, 1323–1349.

7 Brites, C. D. S.; Lima, P. P.; Silva, N. J. O.; Millán, A.; Amaral, V. S.; Palacio, F.; Carlos, L. D. Thermometry at the Nanoscale. *Nanoscale* **2012**, *4*, 4799–4829.

8 Haase, M.; Schäfer, H. Upconverting Nanoparticles. *Angew. Chem., Int. Ed.* **2011**, *50*, 5808–5829.

9 Auzel, F. Upconversion and Anti-Stokes Processes with f and d Ions in Solids. *Chem. Rev.* **2004**, *104*, 139–173.

10 Judd, B. R. Optical Absorption Intensities of Rare-Earth Ions. *Phys. Rev.* **1962**, *127*, 750–761.

11 Ofelt, G. S. Intensities of Crystal Spectra of Rare-Earth Ions. *J. Chem. Phys.* **1962**, *37*, 511–520.

12 Dijk, J. M. F.; Schuurmans, M. F. H. On the Nonradiative and Radiative Decay Rates and A Modified Exponential Energy Gap Law for 4f-4f Transitions in Rare-Earth Ions. *J. Chem. Phys.* **1983**, *78*, 5317–5323.

13 He, G. S.; Tan, L. S.; Zheng, Q.; Prasad, P. N. Multiphoton Absorbing Materials: Molecular Designs, Characterizations, and Applications. *Chem. Rev.* **2008**, *108*, 1245–1330.

14 Chen, G.; Ohulchanskyy, T. Y.; Kumar, R.; Ågren, H.; Prasad, P. N. Ultrasmall Monodisperse $NaYF_4$:Yb^{3+}/Tm^{3+} Nanocrystals with Enhanced Near-Infrared to Near-Infrared Upconversion Photoluminescence. *ACS Nano* **2010**, *4*, 3163–3168.

15 Chen, G.; Ohulchanskyy, T. Y.; Liu, S.; Law, W. C.; Wu, F.; Swihart, M. T.; Ågren, H.; Prasad, P. N. Core/Shell $NaGdF_4$:Nd^{3+}/$NaGdF_4$ Nanocrystals with Efficient Near-Infrared to Near-Infrared Downconversion Photoluminescence for Bioimaging Applications. *ACS Nano* **2012**, *6*, 2969–2977.

16 Krämer, K.; Biner, D.; Frei, G.; Güdel; Hehlen, M.; Lüthi, S. Hexagonal Sodium Yttrium Fluoride Based Green and Blue Emitting Upconversion Phosphors. *Chem. Mater.* **2004**, *16*, 1244–1251.

17 Patra, A.; Friend, C. S.; Kapoor, R.; Prasad, P. N. Effect of Crystal Nature on Upconversion Luminescence in Er^{3+}:ZrO_2 Nanocrystals. *Appl. Phys. Lett.* **2003**, *83*, 284–286.

18 Chen, G.; Liu, H.; Liang, H.; Somesfalean, G.; Zhang, Z. Upconversion Emission Enhancement in Yb^{3+}/Er^{3+}-Codoped Y_2O_3 Nanocrystals by Tridoping with Li^+ Ions. *J. Phys. Chem. C* **2008**, *112*, 12030–12036.

19 Chen, G.; Ohulchanskyy, T. Y.; Kachynski, A.; Ågren, H.; Prasad, P. N. Intense Visible and Near-Infrared Upconversion Photoluminescence in Colloidal $LiYF_4$:Er^{3+} Nanocrystals under Exciation at 1490 nm. *ACS Nano* **2011**, *5*, 4981–4986.

20 Boyer, J.; Veggel, F. Absolute Quantum Yield Measurements of Colloidal $NaYF_4$:Er^{3+},Yb^{3+} Upconverting Nanoparticles. *Nanoscale* **2010**, *2*, 1417–1419.

21 Chen, G.; Shen, J.; Ohulchanskyy, T. Y.; Patel, N. J.; Kuikov, A.; Li, Z.; Song, J.; Pandey, R. K.; Ågren, H.; Prasad, P. N. (α-$NaYbF_4$:Tm^{3+})/CaF_2 Core/Shell Nanoparticles with Efficient Near-Infrared to Near-Infrared Upconversion for High-Contrast Deep Tissue Bioimaging. *ACS Nano* **2012**, *6*, 8280–8287.

22 Chen, G.; Qiu, H.; Fan, R.; Hao, S.; Tan, S.; Yang, C.; Han, G. Lanthanide-Doped Ultrasmall Yttrium Fluoride Nanoparticles with Enhanced Multicolor Upconversion Photoluminescence. *J. Mater. Chem.* **2012**, *38*, 20190–20196.

23 Qiu, H.; Chen, G.; Sun, L.; Hao, S.; Han, G.; Yang, C. Ethylenediaminetetraacetic Acid (EDTA)-Controlled Synthesis of Multicolor Lanthanide Doped $BaYF_5$ Upconversion Nanocrystals. *J. Mater. Chem.* **2011**, *21*, 17202–17208.

24 Chen, G.; Ohulchanskyy, T. Y.; Law, W. C.; Ågren, H.; Prasad, P. N. Monodisperse $NaYbF_4$:Tm^{3+}/$NaGdF_4$ Core/Shell Nanocrystals with Near-Infrared to Near-Infrared Upconversion Photoluminescence and Magnetic Resonance Properties. *Nanoscale* **2011**, *3*, 2003–2008.

25 Nyk, M.; Kumar, R.; Ohulchanskyy, T. Y.; Bergey, E. J.; Prasad, P. N. High Contrast in Vitro and in Vivo Photoluminescence Bioimaging Using Near Infrared to Near Infrared Upconversion in Tm^{3+} and Yb^{3+} Doped Fluoride Nanophosphors. *Nano Lett.* **2008**, *8*, 3834–3838.

26 Kumar, R.; Nyk, M.; Ohulchanskyy, T. Y.; Flask, C. A.; Prasad, P. N. Combined Optical and MR Bioimaging Using Rare Earth Ion Doped $NaYF_4$ Nanocrystals. *Adv. Funct. Mater.* **2009**, *19*, 853–859.

27 Bogdan, N.; Vetrone, F.; Ozin, G. A.; Capobianco, J. A. Synthesis of Ligand-Free Colloidally Stable Water Dispersible Brightly Luminescent Lanthanide-Doped Upconverting Nanoparticles. *Nano Lett.* **2011**, *11*, 835–840.

28 Kim, W. J.; Nyk, M.; Prasad, P. N. Color-Coded Multilayer Photopatterned Microstructures Using Lanthanide (III) Ion Co-Doped $NaYF_4$ Nanoparticles with Upconversion Luminescence for Possible Applications in Security. *Nanotechnology* **2009**, *20* (18), No. 185301.

29 Yuan, C.; Chen, G. Y.; Prasad, P. N.; Ohulchanskyy, T. Y.; Tian, H.; Sun, L. C.; Ågren, H. Use of Colloidal Upconversion Nanocrystals to Energy Relay Solar Cell Light Harvesting in the Near Infrared Region. *J. Mater. Chem.* **2012**, *22*, 16709–16713.